

Atomic and Electronic Structures of WTe_2 Probed by High Resolution Electron Microscopy and *ab Initio* Calculations

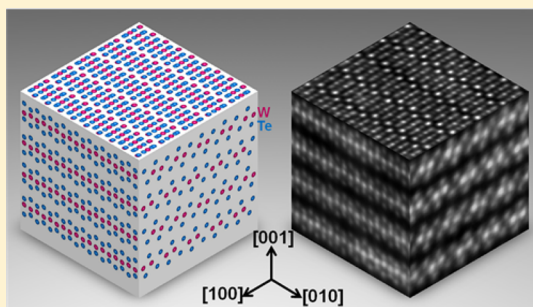
Ning Lu,[†] Chenxi Zhang,[†] Chia-Hui Lee,^{‡,||} Juan Pablo Oviedo,[†] Minh An T. Nguyen,^{§,||} Xin Peng,[†] Robert M. Wallace,[†] Thomas E. Mallouk,^{§,||} Joshua A. Robinson,^{‡,||} Jinguo Wang,[†] Kyeongjae Cho,[†] and Moon J. Kim^{*,†}

[†]Department of Materials Science and Engineering, The University of Texas at Dallas, Richardson, Texas 75080, United States

[‡]Department of Materials Science and Engineering, [§]Department of Chemistry, and ^{||}Center for 2-Dimensional and Layered Materials, The Pennsylvania State University, University Park, Pennsylvania 16802, United States

S Supporting Information

ABSTRACT: Transition metal dichalcogenides (TMDs) are a class of two-dimensional (2D) materials that have attracted growing interest because of their unique electronic and optical properties. Under ambient conditions, most TMDs generally exhibit 2H or 1T structures. Unlike other group VIb TMDs, bulk crystals and powders of WTe_2 exist in a distorted 1T structure (Td) at room temperature and have semimetallic properties. There is so far a lack of direct atom-by-atom visualization, limiting our understanding of this distorted 2D layered material system. We present herein atomic resolution images of Td structured WTe_2 . The Td structure can be distinguished in the three major orientations along the [100], [010], and [001] zone axes. Subtle structural distortions are detected by atomic resolution imaging, which match well with the optimized structure relaxed by *ab initio* calculations. The calculations also showed that both crystal field splitting and charge density wave (CDW) interactions contribute to the stabilization of WTe_2 . However, the CDW interaction dominates and leads the Td- WTe_2 to be the most stable structure. The combined atomic resolution STEM and *ab initio* study on WTe_2 provided the basis for understanding the correlations between atomic structure and electronic properties in Td structured TMD materials.



INTRODUCTION

Transition metal dichalcogenides (TMDs) MX_2 , where M is a transition metal (Mo, W, Hf, etc.) and X is a chalcogen (S, Se, and Te), are a class of two-dimensional (2D) materials that have attracted growing interest because of their unique electronic and optical properties.^{1–3} Recent reports have explored the crystal structures, syntheses, and electronic properties of TMD systems using both experimental and theoretical techniques.⁴ These studies suggest that the absence of dangling bonds⁵ and the wide range of band gaps (from 3.5 to <1 eV)⁶ make TMD materials attractive in practical devices, such as field effect transistors^{2,7,8} and photosensors.^{9,10}

TMDs have layered structures with an X–M–X atomic stacking sequence in each layer. When the M atoms are coordinated by a trigonal prism of X atoms, the structure is defined as the 2H phase,¹¹ as shown in Figure 1a. There are two X–M–X layers in each unit cell of the 2H structure. Group VIb TMDs that adopt the 2H structure, such as MoS_2 and WS_2 , are usually semiconductors with band gaps between 1 and 2 eV.^{1,6} When one X layer is shifted such that the metal becomes octahedrally coordinated, the structure is referred to as the 1T phase,¹¹ as shown in Figure 1b. In this case there is only one X–M–X layer in the unit cell. The 1T structure TMDs cover a broad spectrum of electrical properties, from insulators such as

HfS_2 , through semiconductors such as $HfSe_2$, to metals such as TiS_2 .¹¹ Under ambient conditions, most TMDs exist in 2H or 1T structures. Unlike other group VIb TMDs, bulk crystals and powders of WTe_2 are generally found in a distorted 1T structure (Td, also called 1T') at room temperature and have semimetallic properties.^{12–18} Reports of the 2H (semiconducting) phase of WTe_2 appear to be limited to the powder synthesis work by Champion¹⁹ and have been summarized in the review by Wilson and Yoffe.¹¹ *Ab initio* calculations have been used to investigate the electronic structure of WTe_2 , and it has been found they exhibit semimetal properties which arise from the small electron and hole pockets along the Γ –X direction.^{15,20} Another possible explanation is that there is a 0.5 eV overlap of Te 5p and W 5d-like bands along Γ –Y, and the low conductivity of WTe_2 is due to the low density of states at the Fermi level.²¹ Angle-resolved photoemission spectroscopy (ARPES) was used to confirm the electronic structure of WTe_2 , and it was found that carrier compensation would be the primary source of formation of similar-sized electron and hole pockets.²² Very recently, an extremely large positive magneto-

Received: January 30, 2016

Revised: April 3, 2016

Published: April 5, 2016

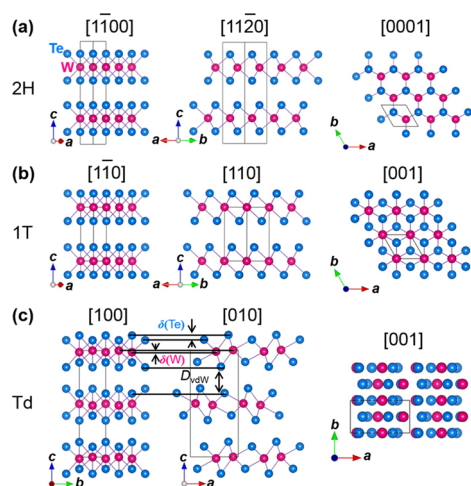


Figure 1. Schematic models of WTe_2 with 2H, 1T, and Td structures optimized by ab initio calculations in $[1\bar{1}00]$ ($[1\bar{1}0]$, $[100]$), $[11\bar{2}0]$ ($[110]$, $[010]$), and $[0001]$ ($[001]$, $[001]$) orientations, respectively. Pink atoms represent tungsten and blue atoms tellurium.

resistance at low temperatures has been discovered in the nonmagnetic Td structure WTe_2 .²⁰ Although electrical and magnetic studies of WTe_2 as a novel material system have been carried out, there is so far a lack of direct atom-by-atom visualization, limiting our understanding of this distorted 2D layered material system. Moreover, the correlation between the structure and electronic properties in WTe_2 also has not been well understood yet. Here we have combined atomic imaging and ab initio calculations to reveal the atomic and electronic structures of Td- WTe_2 . Furthermore, charge density wave (CDW) is used to understand the atomic structure and electronic property correlations in WTe_2 .

EXPERIMENTAL METHODS

Synthesis of WTe_2 Flakes. WTe_2 bulk crystals were produced by the chemical vapor transport method using bromine as the transport agent. The details of the synthetic method can be found in the previous work.¹⁸ The X-ray diffraction (XRD) patterns of the synthesized WTe_2 flakes confirmed the bulk WTe_2 crystals are orthorhombic space group $Pmn2_1$, with Td structure.¹⁸

Atomic Imaging and Image Simulations. Transmission electron microscopic (TEM) cross-sectional samples were made by using a FEI Nova 200 dual-beam focused ion beam scanning electron microscope (FIB/SEM) by the lift-out method. In the FIB, SiO_2 and Pt layers were deposited to protect the region of interest during focused ion beam milling. Atomic high angle angular dark field scanning transmission electron microscopy (HAADF-STEM) was performed in a JEOL ARM200F microscope with a probe aberration corrector (CEOS GmbH) operated at 200 kV. HAADF-STEM images based on the optimized atomic structure were simulated using the xHREM software package.

Ab Initio Calculations. The calculations were performed by using the Vienna Ab initio Simulation Package (VASP).²³ The projector-augmented wave (PAW) pseudopotential²⁴ is adopted, and the generalized gradient approximation (GGA) of Perdew–Burke–Ernzerhof (PBE) functionals were used to describe the exchange–correlation.²⁵ Spin–orbit coupling is included for the band structure calculations along high symmetry points in the Brillouin zone (BZ).

In this work, the structures of all the TMDs studied were optimized based on both 2H and 1T bulk crystal structures, with the remnant force on each atom below $0.01 \text{ eV}/\text{\AA}$ as the stopping criterion for ionic relaxation. The Grimme-D3 correction, to correct the van der Waals (vdW) interaction between layers, is included in order to get a better optimized crystal structure of bulk WTe_2 .^{26,27} The Monkhorst–Pack k -point sampling in BZ is Γ -centered with $6 \times 12 \times 4$ and $24 \times 24 \times 8$ meshes in ionic and electronic optimization, respectively.²⁸ The energy cutoff is 500 eV. The electronic optimization was stopped when the total energies of neighboring loops differed by less than 10^{-4} eV .

RESULTS AND DISCUSSION

Figure 1 shows schematic models of WTe_2 in the 2H, 1T, and Td structures optimized by ab initio calculations in $[1\bar{1}00]$ ($[1\bar{1}0]$, $[100]$), $[11\bar{2}0]$ ($[110]$, $[010]$), and $[0001]$ ($[001]$, $[001]$) orientations, respectively. The Td structure can be clearly distinguished in its three major orientations. In these layered TMD compounds, metal layers are sandwiched between adjacent chalcogenide layers; this dichalcogenide sandwich stacks along the c -axis of the unit cell, with van der Waals bonding between layers. Unlike the 1T and 2H structures, Td- WTe_2 contains noncoplanar atomic layers of both W and Te. This puckering of layers is caused by an additional structural distortion: tungsten chains are formed within the tellurium layers along the b -axis of the orthorhombic unit cell as shown in Figure 1c, $[001]$ orientation.

Figure 2 shows the local bonding characteristics of 2H-, 1T-, and Td- WTe_2 . In 2H-, 1T-, and Td- WTe_2 , the W atoms are all

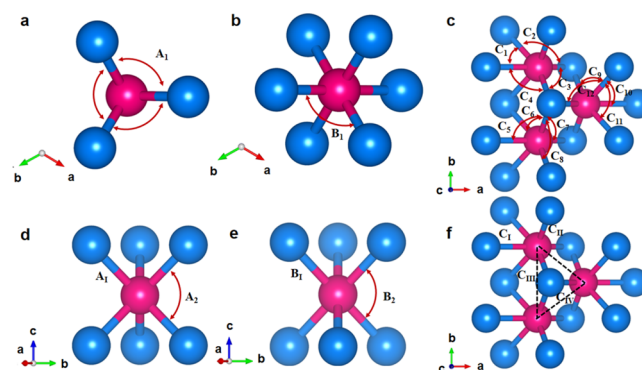


Figure 2. Different local bonding characteristics in bulk 2H- (a, d), 1T- (b, e), and Td- WTe_2 (c, f). The bond angles in the 2H, 1T, and Td structures are indicated by A_1 , B_1 – B_3 , and C_1 – C_{12} . The bond lengths in the 2H, 1T, and Td structures are indicated by A_1 , B_1 , and C_1 – C_{1V} . The dashed line triangle indicates the W–W bonding in bulk Td- WTe_2 .

covalently bonded with neighboring Te atoms forming a sandwich-like trigonal prismatic structure. Comparing 2H with 1T, the upper triangle of the prism is rotated by about 60° , which can be seen in Figure 2a,b. Two antiparallel equilateral triangles are located above and below the W atom layer in the 1T structure, whereas in the 2H structure the two equilateral triangles of Te are parallel. The W–Te bond lengths in 2H structure are quite similar to those in the 1T structure, which are marked by A_1 and B_1 in Table 1. The W–W bond lengths are also very similar in the 1T and 2H structures, at 3.51 and 3.48 \AA , respectively. The bond angles between W and two Te atoms in the same layer are quite similar in the 1T and 2H

Table 1. Bond Angles and Bond Lengths in Bulk 2H-, 1T-, and Td-WTe₂

bond angle (deg)	2H-WTe ₂	bond angle (deg)	1T-WTe ₂	bond angle (deg)	Td-WTe ₂	bond angle (deg)	Td-WTe ₂
A ₁	80.25	B ₁	78.80	C ₁	77.18	C ₇	117.35
A ₂	83.82	B ₂	101.20	C ₂	83.14	C ₈	79.41
				C ₃	117.35	C ₉	98.53
				C ₄	81.07	C ₁₀	77.13
				C ₅	81.07	C ₁₁	75.69
				C ₆	98.28	C ₁₂	83.36
bond length (Å)	2H-WTe ₂	bond length (Å)	1T-WTe ₂	bond length (Å)	Td-WTe ₂	bond length (Å)	Td-WTe ₂
A ₁	2.72	B ₁	2.74	C ₁	2.82	C _{III}	3.46
W–W	3.51	W–W	3.48	C _{II}	2.71	C _{IV}	2.84

structures (A₁ 80.25° and B₁ 78.80°). In contrast, the bond angles between W and Te atoms in different layers are different in the 2H and 1T structures because of the rotation of Te triangles in the 1T structure (A₂ is 83.82° and B₂ is 101.20°). In the Td structure, the W atoms are shifted from the center of the prisms forming a zigzag chain along the *b*-axis which can be seen in Figure 2f (black triangle). One pair of W–W bonds becomes shorter while the other becomes longer because of the existence of charge density wave distortion.²⁹ The W–W bond length is much shorter than that in the 2H and 1T structures, as shown in Table 1. The length of one W–W bond (C_{II} in Table 1, 2.71 Å) is close to that in tungsten metal (2.74 Å). Due to the shift of W atoms, the bond lengths and bond angles of Td-WTe₂ are modified compared to the 1T structure. Three W–Te bonds are shortened (C_{II}), and the other three are stretched (C_I). The Te plane is crumpled due to the distortion and forming a zigzag shape, as shown in Figure 1c. Because of the displacement of W atoms from the center, the original octahedral symmetry is broken and the octahedron formed by W and its six neighboring Te's are distorted causing the random distribution of bond angles between W and Te atoms (shown in Table 1).

The vertical shift along the *c*-axis of W and Te atoms is an obvious feature in the [100] and [010] views of the structure, as shown in Figure 1c. These atoms form zigzag-like planes, especially the Te layers which form a buckled van der Waals gap. We define the vertical displacement between the nearest neighbor W and Te atoms as $\delta(W)$ and $\delta(\text{Te})$, as indicated in Figure 1c. The size of the buckled van der Waals gap (D_{vdW} , in Figure 1c) is expressed as the closest tellurium–tellurium vertical distance. D_c denotes the lattice parameter of the unit cell along the *c*-axis. We can obtain the relative vertical displacement of nearest neighbor W and Te atoms in the Td unit cell by using $\Delta(W) = \delta(W)/D_c$ and $\Delta(\text{Te}) = \delta(\text{Te})/D_c$. In the relaxed Td structure, $D_c = 14.06$ Å, $D_{\text{vdW}} \sim 3.47$ Å, $\delta(W) \sim 0.21$ Å, $\Delta(W) \sim 1.5\%$, $\delta(\text{Te}) \sim 0.63$ Å, and $\Delta(\text{Te}) \sim 4.5\%$. These subtle structural distortions can be detected by atomic high angle angular dark field (HAADF) scanning transmission electron microscopy (STEM) imaging as shown below.

Figure 3 shows experimental HAADF-STEM atomic images of chemical vapor transport (CVT) grown Td structure WTe₂ in [100], [010], and [001] orientations. In order to reduce the noise levels and to improve the accuracy of the image analysis, a probe deconvolution algorithm based on maximum entropy methods was applied to the images to remove the contribution of the tails of the focused electron probe to the column intensity.³⁰ The raw images are shown in the Supporting Information, Figure S1. The contrast in HAADF-STEM images is approximately proportional to Z^2 , where Z is the atomic number.³¹ The contrast provides a way to identify different

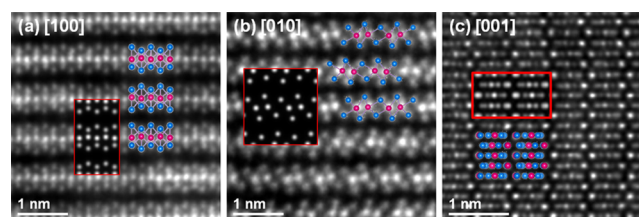


Figure 3. Atomic resolution HAADF-STEM images of CVT grown Td-WTe₂ in the (a) [100], (b) [010], and (c) [001] orientations. The images were probe-deconvoluted for improved visibility. The insets in the red rectangles are the simulated STEM images based on the optimized Td-WTe₂ structure. The corresponding calculated atomic models are inset as well.

atomic species, in so-called Z-contrast imaging. Using HAADF, the W and Te atomic columns are clearly distinguished, as shown in Figure 3. In [100] (Figure 3a) and [010] (Figure 3b) orientations, the Te–W–Te sandwich stacks can be discerned clearly. All atomic columns along these two viewing directions can be distinguished as pure W and Te columns. The bright spots in the middle of the dichalcogenide sandwich are W ($Z = 74$) atomic columns, and the dim spots are the Te ($Z = 52$) columns. In the [001] orientation (Figure 3c), there are some mixed atomic columns. In the [001] projection of the Td-WTe₂ unit cell, as shown in the inset of Figure 3c and Figure 1, the bottom left, top left, and middle right atomic columns contain one W and one Te atom, and the other spots are occupied by either one W or one Te atom. Therefore, the brightest spots in Figure 3c, which form a zigzag chain, are the mixed W/Te atomic columns. The second brightest spots are the pure W atomic columns. Plan view STEM images of Td structure TMDs are widely different from those of the 1T and 2H structures with their hexagonal honeycomb patterns, as shown in Figure 1.

The vertical displacement of W and Te atoms is clearly observed in the [100] and [010] side view orientations as shown in Figure 3a,b. The buckled Te layers with their obvious vertical shift can be clearly seen. The zigzag of W layers directly reflects the tiny displacement of W atoms in both Figure 3a and 3b. The relative vertical displacement of nearest neighbor W and Te atoms in 20 unit cells, 10 cells each for [100] and [010] orientations, were measured. $\Delta(W) = 2.0 \pm 0.5\%$; $\Delta(\text{Te}) = 4.7 \pm 0.3\%$. These experimental measurements fit well with the calculated results, 1.5 and 4.5%, respectively. The subtle atomic distortions have been successfully captured by Cs-corrected STEM imaging. The pair of bright spots in Figure 3b, i.e. the W atomic columns, also indicates the horizontal off-center distortion of W atoms. To further compare the calculated structure with the experimental results, HAADF-STEM image

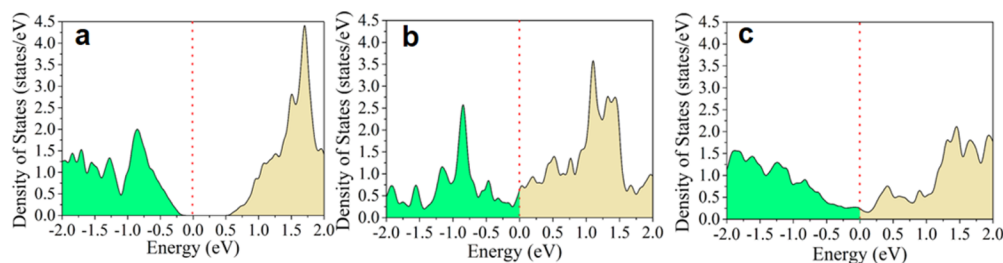


Figure 4. Density of states of d orbitals of W atoms in bulk (a) 2H-, (b) 1T-, and (c) Td-WTe₂.

simulations were carried out. HAADF-STEM images based on the optimized Td atomic structure were simulated along the [100], [010], and [001] zone axes, as shown in the insets with red borders in Figure 3, respectively. The simulated images fit well with experimental images, confirming the reliability of the calculated structure of Td-WTe₂, which also demonstrates that the Grimme-D3 correction of vdW interaction works well in such distorted layered TMD materials.

The good consistency between simulated image based on DFT calculation and the experimental atomic resolution STEM images establishes the bridge to correlate the atomic structure and electronic properties in WTe₂. To explain the structural stability of the WTe₂ system, two theories are introduced and discussed to investigate the structure–property relation in WTe₂. One is the crystal field splitting (CFS), a model used to describe the breaking of degeneracies of transition metal d orbitals in terms of the distribution of surrounding anions. In many TMDs, the conduction and valence bands close to the Fermi level are mainly composed by metal d and chalcogen p orbitals. In different metal–chalcogen coordination geometries, various hybridizations of these states exist and thus different crystal field splittings are generated. In the 1T structure in which the metal is octahedrally coordinated, the d orbitals split into the two energy levels t_{2g} (d_{xy} , d_{yz} , d_{xz}) and e_g ($d_x^2 - y^2$ and d_z^2). In the 2H structure, the metal is in trigonal prismatic coordination, and the d orbitals split into three groups: d_{xz} , d_{yz} , $d_x^2 - y^2$, d_{xy} ; and d_z^2 . The d_z^2 orbital has the lowest energy in this geometry, as shown in the Supporting Information, Figure S2. The diverse electronic properties of TMDs originated from filling metal d orbital electrons to different levels when the transition metal varies from group IV to group X.⁴ In the 2H structure of group VI TMDs, the d_z^2 orbital is filled and a gap of ~ 0.75 eV exists between d_z^2 and the unoccupied upper levels making it a semiconductor (shown in Figure 4a). The fully occupied d_z^2 orbital stabilizes the 2H structure of WTe₂ more than the partially filled t_{2g} orbital in the 1T structure.⁶ Our DFT calculation shows the total energy of WTe₂ was reduced by 0.56 eV in going from the 1T to the 2H structure.

The other significant mechanism is the existence of charge density wave. A charge density wave is a periodic modulation of electronic charge density, which is accompanied by a periodic lattice distortion (PLD). Electronically driven PLDs have been observed in several TMDs (including 1T-TaSe₂, 1T-TaS₂, and NbSe₂) at low temperatures.^{32–36} Because of the existence of CDW, the W atoms are displaced from their ideal octahedral sites along the *a*-axis and form zigzag chains along the *b*-axis. This is comparable to the Peierls transition in a one-dimensional metal chain in which a gap opening is observed due to the dimerization of metal atoms and the periodicity change.³⁷ However, the band gap opening of one-dimensional Peierls distortion along the *b*-axis in Td-WTe₂ is suppressed

since it maintains the regular periodicity. Although the distortion is not large enough to open a gap, it still results in the reduction of density of states around the Fermi level (−0.5 to 0.5 eV) in Td-WTe₂ compared to 1T-WTe₂ (shown in Figure 4b,c). The reduced density of states leads the Td-WTe₂ to be semimetallic rather than metallic in 1T-WTe₂. Band structures of Td-, 2H-, and 1T-WTe₂ were calculated and shown in the Supporting Information, Figures S3, S4, and S5, respectively. It can be observed that, close to the Fermi level (at Γ and Z), only a few occupied bands cross the Fermi level (Supporting Information, Figure S3). This is consistent with the low density of states near the Fermi level supporting the existence of the CDW.

Apart from the impact on the electronic properties, the CDW distortion also affects the energetic stability of Td-WTe₂. The distortion can cause the increase in elastic energy, but this energy increase can be compensated by the reduction of electronic energy induced by the CDW. In other words, the existence of CDW makes Td-WTe₂ more stable than 1T-WTe₂. Ab initio calculations show that the energies of 2H-, 1T-, and Td-WTe₂ are in the sequence E_{1T} (−18.88 eV) > E_{2H} (−19.44 eV) > E_{Td} (−19.52 eV). CDW induces an energy reduction of 0.64 eV in the Td structure with reference to the 1T structure while the CFS only results in an energy reduction of 0.56 eV in the 2H structure. This indicates that the CDW distortion dominated energy reduction make the Td structure to be the most stable. Furthermore, the small energy difference between the Td and 2H structures of WTe₂ shows its rich applications in phase transition devices which is consistent with previous works.^{38,39}

CONCLUSIONS

In this work, we have reported directly visualized atomic images of the distorted structural WTe₂ for the first time. The Td structure can be distinguished in the three major orientations, along the [100], [010], and [001] zone axes. These subtle structural distortions are clearly detected by atomic resolution imaging, and match well with the optimized structure predicted by ab initio calculations with vdW interaction correction. The ab initio calculations also showed that both crystal field splitting and charge density wave interactions contribute to the stabilization of WTe₂. However, the CDW interaction dominates and leads Td-WTe₂ to be the most stable structure. The calculated density of states and band structure of Td-WTe₂ show that it is semimetallic, and this property originates from the CDW and accompanying period lattice distortion. The combined atomic resolution STEM and ab initio study on WTe₂ provided direct proof of correlation between the atomic structure and electronic structure in TMDs and pave the way to the controlled phase engineering of desired structures and electrical behaviors in future TMD device applications.

■ ASSOCIATED CONTENT

■ Supporting Information

The Supporting Information is available free of charge on the ACS Publications website at DOI: 10.1021/acs.jpcc.6b01044.

Figures S1–S5 including raw HAADF-STEM images; energy level splitting of d orbitals of W; band structures of Td-, 2H-, and 1T-WSe₂ (PDF)

■ AUTHOR INFORMATION

Corresponding Author

*Tel.: 972-883-6635. Fax: 972-883-5725. E-mail: moonkim@utdallas.edu.

Present Address

N.L.: Micron Technology, Inc., Boise, Idaho 83716, United States.

Author Contributions

The manuscript was written through contributions of all authors. All authors have given approval to the final version of the manuscript. N.L. and C.Z. contributed equally.

Notes

The authors declare no competing financial interest.

■ ACKNOWLEDGMENTS

This work was supported by the Center for Low Energy Systems Technology (LEAST), one of six centers supported by the STARnet phase of the Focus Center Research Program (FCRP), a Semiconductor Research Corporation program sponsored by MARCO and DARPA, and by the Louis Beecherl, Jr., endowment funds. M.A.T.N. and T.E.M. acknowledge support from U.S. Army Research Office MURI Grant W911NF-11-1-0362.

■ REFERENCES

- (1) Wang, Q. H.; Kalantar-Zadeh, K.; Kis, A.; Coleman, J. N.; Strano, M. S. Electronics and Optoelectronics of Two-Dimensional Transition Metal Dichalcogenides. *Nat. Nanotechnol.* **2012**, *7*, 699–712.
- (2) Radisavljevic, B.; Radenovic, A.; Brivio, J.; Giacometti, V.; Kis, A. Single-Layer MoS₂ Transistors. *Nat. Nanotechnol.* **2011**, *6*, 147–150.
- (3) Levi, R.; Bitton, O.; Leitus, G.; Tenne, R.; Joselevich, E. Field-Effect Transistors Based on WS₂ Nanotubes with High Current-Carrying Capacity. *Nano Lett.* **2013**, *13*, 3736–3741.
- (4) Chhowalla, M.; Shin, H. S.; Eda, G.; Li, L. J.; Loh, K. P.; Zhang, H. The Chemistry of Two-Dimensional Layered Transition Metal Dichalcogenide Nanosheets. *Nat. Chem.* **2013**, *5*, 263–275.
- (5) Jena, D. Tunneling Transistors Based on Graphene and 2-D Crystals. *Proc. IEEE* **2013**, *101*, 1585–1602.
- (6) Gong, C.; Zhang, H. J.; Wang, W. H.; Colombo, L.; Wallace, R. M.; Cho, K. J. Band Alignment of Two-Dimensional Transition Metal Dichalcogenides: Application in Tunnel Field Effect Transistors. *Appl. Phys. Lett.* **2013**, *103*, 053513.
- (7) Lam, K. T.; Cao, X.; Guo, J. Device Performance of Heterojunction Tunneling Field-Effect Transistors Based on Transition Metal Dichalcogenide Monolayer. *IEEE Electron Device Lett.* **2013**, *34*, 1331–1333.
- (8) Ilatkhameneh, H.; Tan, Y.; Novakovic, B.; Klimeck, G.; Rahman, R.; Appenzeller, J. Tunnel Field-Effect Transistors in 2D Transition Metal Dichalcogenide Materials. *IEEE J. Exploratory Solid-State Comput. Devices Circuits* **2015**, *1*, 12–18.
- (9) Perea-Lopez, N.; Elias, A. L.; Berkdemir, A.; Castro-Beltran, A.; Gutierrez, H. R.; Feng, S. M.; Lv, R. T.; Hayashi, T.; Lopez-Urias, F.; Ghosh, S.; et al. Photosensor Device Based on Few-Layered WS₂ Films. *Adv. Funct. Mater.* **2013**, *23*, 5511–5517.

(10) Yin, Z. Y.; Li, H.; Li, H.; Jiang, L.; Shi, Y. M.; Sun, Y. H.; Lu, G.; Zhang, Q.; Chen, X. D.; Zhang, H. Single-Layer MoS₂ Phototransistors. *ACS Nano* **2012**, *6*, 74–80.

(11) Wilson, J. A.; Yoffe, A. D. Transition Metal Dichalcogenides Discussion and Interpretation of Observed Optical, Electrical and Structural Properties. *Adv. Phys.* **1969**, *18*, 193–335.

(12) Brixner, L. H. Preparation and Properties of the Single Crystalline AB₂-Type Selenides and Tellurides of Niobium, Tantalum, Molybdenum and Tungsten. *J. Inorg. Nucl. Chem.* **1962**, *24*, 257–263.

(13) Brown, B. E. Crystal Structures of WTe₂ and High-Temperature MoTe₂. *Acta Crystallogr.* **1966**, *20*, 268–274.

(14) Kabashima, S. Electrical Properties of Tungsten-Ditelluride WTe₂. *J. Phys. Soc. Jpn.* **1966**, *21*, 945–948.

(15) Dawson, W. G.; Bullett, D. W. Electronic-Structure and Crystallography of MoTe₂ and WTe₂. *J. Phys. C: Solid State Phys.* **1987**, *20*, 6159–6174.

(16) Callanan, J. E.; Hope, G. A.; Weir, R. D.; Westrum, E. F. Thermodynamic Properties of Tungsten Ditelluride (WTe₂) I. The Preparation and Lowtemperature Heat-Capacity at Temperatures from 6 to 326 K. *J. Chem. Thermodyn.* **1992**, *24*, 627–638.

(17) O'Hare, P. A. G.; Hope, G. A. Thermodynamic Properties of Tungsten Ditelluride (WTe₂) II. Standard Molar Enthalpy of Formation at the Temperature 298.15 K. *J. Chem. Thermodyn.* **1992**, *24*, 639–647.

(18) Lee, C.-H.; Silva, E. C.; Calderin, L.; Nguyen, M. A. T.; Hollander, M. J.; Bersch, B.; Mallouk, T. E.; Robinson, J. A. Tungsten Ditelluride: A Layered Semimetal. *Sci. Rep.* **2015**, *5*, 10013.

(19) Champion, J. A. Some Properties of (Mo,W) (Se,Te)₂. *Br. J. Appl. Phys.* **1965**, *16*, 1035–1037.

(20) Ali, M. N.; Xiong, J.; Flynn, S.; Tao, J.; Gibson, Q. D.; Schoop, L. M.; Liang, T.; Haldolaarachchige, N.; Hirschberger, M.; Ong, N. P.; et al. Large, Non-Saturating Magnetoresistance in WTe₂. *Nature* **2014**, *514*, 205–208.

(21) Augustin, J.; Eyert, V.; Boker, T.; Frentrup, W.; Dwelk, H.; Janowitz, C.; Manzke, R. Electronic Band Structure of the Layered Compound Td-WTe₂. *Phys. Rev. B: Condens. Matter Mater. Phys.* **2000**, *62*, 10812–10823.

(22) Pletikoscic, I.; Ali, M. N.; Fedorov, A. V.; Cava, R. J.; Valla, T. Electronic Structure Basis for the Extraordinary Magnetoresistance in WTe₂. *Phys. Rev. Lett.* **2014**, *113*, 216601.

(23) Kresse, G.; Furthmüller, J. Efficient Iterative Schemes for ab initio Total-Energy Calculations Using a Plane-Wave Basis Set. *Phys. Rev. B: Condens. Matter Mater. Phys.* **1996**, *54*, 11169–11186.

(24) Kresse, G.; Joubert, D. From Ultrasoft Pseudopotentials to the Projector Augmented-Wave Method. *Phys. Rev. B: Condens. Matter Mater. Phys.* **1999**, *59*, 1758–1775.

(25) Perdew, J. P.; Burke, K.; Ernzerhof, M. Generalized Gradient Approximation Made Simple. *Phys. Rev. Lett.* **1996**, *77*, 3865–3868.

(26) Grimme, S.; Antony, J.; Ehrlich, S.; Krieg, H. A Consistent and Accurate Ab Initio Parametrization of Density Functional Dispersion Correction (DFT-D) for the 94 Elements H-Pu. *J. Chem. Phys.* **2010**, *132*, 154104.

(27) Grimme, S.; Ehrlich, S.; Goerigk, L. Effect of the Damping Function in Dispersion Corrected Density Functional Theory. *J. Comput. Chem.* **2011**, *32*, 1456–1465.

(28) Monkhorst, H. J.; Pack, J. D. Special Points for Brillouin-Zone Integrations. *Phys. Rev. B* **1976**, *13*, 5188–5192.

(29) Monceau, P. Electronic Crystals: An Experimental Overview. *Adv. Phys.* **2012**, *61*, 325–581.

(30) Ishizuka, K.; Abe, E. Improvement of Spatial Resolution of STEM-HAADF Image by Maximum-Entropy and Richardson-Lucy Deconvolution. *Proceedings of the 13th European Microscopy Congress*; Belgian Society for Microscopy: Liège, Belgium, 2004; Vol. 1, p 117.

(31) Hartel, P.; Rose, H.; Dinges, C. Conditions and Reasons for Incoherent Imaging in STEM. *Ultramicroscopy* **1996**, *63*, 93–114.

(32) Hollander, M. J.; Liu, Y.; Lu, W. J.; Li, L. J.; Sun, Y. P.; Robinson, J. A.; Datta, S. Electrically Driven Reversible Insulator-Metal Phase Transition in 1T-TaS₂. *Nano Lett.* **2015**, *15*, 1861–1866.

(33) Castro Neto, A. H. Charge Density Wave, Superconductivity, and Anomalous Metallic Behavior in 2D Transition Metal Dichalcogenides. *Phys. Rev. Lett.* **2001**, *86*, 4382–4385.

(34) Rocquefelte, X.; Boucher, F.; Gressier, P.; Ouvrard, G.; Blaha, P.; Schwarz, K. Mo Cluster Formation in the Intercalation Compound LiMoS_2 . *Phys. Rev. B: Condens. Matter Mater. Phys.* **2000**, *62*, 2397–2400.

(35) Wilson, J. A.; Di Salvo, F. J.; Mahajan, S. Charge-Density Waves and Superlattices in the Metallic Layered Transition Metal Dichalcogenides. *Adv. Phys.* **2001**, *50*, 1171–1248.

(36) Zhu, Z. Y.; Cheng, Y. C.; Schwingenschlogl, U. Origin of the Charge Density Wave in 1T-TiSe₂. *Phys. Rev. B: Condens. Matter Mater. Phys.* **2012**, *85*, 245133.

(37) Thorne, R. E. Charge-Density-Wave Conductors. *Phys. Today* **1996**, *49*, 42–47.

(38) KC, S.; Zhang, C.; Hong, S.; Wallace, R. M.; Cho, K. Phase Stability of Transition Metal Dichalcogenide by Competing Ligand Field Stabilization and Charge Density Wave. *2D Mater.* **2015**, *2*, 035019.

(39) Duerloo, K. A. N.; Li, Y.; Reed, E. J. Structural Phase Transitions in Two-Dimensional Mo- and W-Dichalcogenide Monolayers. *Nat. Commun.* **2014**, *5*, 4214.